

# Spectral features in gamma-rays expected from millisecond pulsars

T. Bulik<sup>1</sup>, B. Rudak<sup>2,3</sup> and J. Dyks<sup>2</sup>

<sup>1</sup> *Nicolaus Copernicus Astronomical Center, Bartycka 18, 00716 Warsaw, Poland*

<sup>2</sup> *Nicolaus Copernicus Astronomical Center, Rabiańska 8, 87100 Toruń, Poland*

<sup>3</sup> *TCfA of Nicolaus Copernicus University, Gagarina 11, 87100 Toruń, Poland*

21 March 2018

## ABSTRACT

In the advent of next generation gamma-ray missions, we present general properties of spectral features of high-energy emission above 1 MeV expected for a class of millisecond, low magnetic field ( $\sim 10^9$  G) pulsars. We extend polar-cap model calculations of Rudak & Dyks (1999) by including inverse Compton scattering events in ambient field of thermal X-ray photons and by allowing for two models of particle acceleration. In the range between 1 MeV and a few hundred GeV the main spectral component is due to curvature radiation of primary particles. Synchrotron component due to secondary pairs becomes dominant only below 1 MeV. The slope of the curvature radiation spectrum in the energy range from 100 MeV to 10 GeV strongly depends on the model of longitudinal acceleration, whereas below  $\sim 100$  MeV all slopes converge to a unique value of  $4/3$  (in a  $\nu\mathcal{F}_\nu$  convention). The thermal soft X-ray photons, which come either from the polar cap or from the surface, are Compton upscattered to a domain of the VHE and form a separate spectral component peaking at  $\sim 1$  TeV. We discuss observability of millisecond pulsars by future high energy instruments and present two rankings relevant for GLAST and MAGIC. We point to the pulsar J0437-4715 as a promising candidate for observations.

**Key words:** gamma-rays: theory, observations – pulsars: general

## 1 INTRODUCTION

Millisecond pulsars are thought to be uninteresting as targets for gamma-ray experiments. This opinion partly draws from an argument that typical values of  $B$  (or rather their dipolar components) inferred from  $P$  and  $\dot{P}$  are in the range of  $10^8$  to  $10^9$  G, in contrast with the range of  $10^{11}$  to  $10^{13}$  G for classical pulsars. If gamma-ray radiation is to be a manifestation of magnetospheric activity, it seems quite natural to think of millisecond pulsars in terms of  $B$  as of a scaled-down version of classical pulsars, which by themselves are weak gamma-ray sources; only seven of them have been firmly detected so far (Thompson et al., 1997). Unsuccessful observational campaigns in the past, mainly by *CGRO* instruments e.g. *EGRET* - (Fierro et al., 1995), confirmed this line of thinking. J0437-4715, with one of the highest spin-down fluxes among all pulsars, thus a very promising target, wasn't even included in the *COMPTEL* priority list (Carminana et al., 1995).

However, the ‘scaling-down’ argument becomes unjustified by the results of X-ray observations. Within a sample of some 30 pulsars detected with *ROSAT* and other satellites

there are 9 millisecond objects (Becker & Trümper, 1999) with apparent X-ray properties similar to classical pulsars. In particular, the millisecond pulsars obey the same astonishing relation of Becker & Trümper (1997) between the spin-down luminosity  $L_{\text{sd}}$  and the soft X-ray luminosity  $L_x$  that classical pulsars do. In most cases the X-ray spectra are presumed to be non-thermal in character, but whether they represent low-energy tails of putative gamma-ray emission is not known.

Rather few papers have been dedicated to the question of gamma-rays in the context of millisecond pulsars on theoretical side. Wei et al. (1996) presented broad-band spectra of both pulsed and unpulsed emission expected in their version of outer-gap model. Sturmer & Dermer (1994) offered predictions for gamma-ray luminosity  $L_\gamma$  in some popular models, but that had been done just by scaling-down the values of  $B$  in simple analytical formulae for  $L_\gamma$  derived for classical pulsars. In the framework of polar-cap scenarios, Rudak & Dyks (1998) proposed a modification of the model by Daugherty & Harding (1982). This modification incorporates a contribution of electron-positron pairs to  $L_\gamma$ , which becomes a non-monotonic function of  $B$  (see Figures 7 and

8 of (Dyks, 1998)). One of the consequences of this modification is that expected values of  $L_\gamma$  for millisecond pulsars, including J0437-4715, are typically about one or two orders of magnitude lower than for classical pulsars. Quantitatively similar estimate, though for different reason, comes from a model of Dermer & Sturmer (1994).

However, if the estimates above are correct then some millisecond pulsars, including J0437-4715, should be detected with next-generation experiments, providing thus a testing ground for magnetospheric models relevant for millisecond pulsars. The successor of *EGRET* - *GLAST* - with a possible launch in the year 2005, is expected to have sensitivity above 100 MeV about 30 times higher than *EGRET*, and it will reach high-energy limit at 300 GeV - closing thus for the first time the energy gap between the VHE (very high energy) domain accessible with ground-based Cherenkov techniques and the HE (high energy) domain of satellite experiments (Kamae et al., 1999). Moreover, since we expect the millisecond pulsars to radiate the electromagnetic energy mostly in the range between 10 GeV and 100 GeV, this class of objects should be of interest for the upcoming IAC telescope *MAGIC* (Blanch et al., 1998).

Our aim is to present major spectral features in the energy range above  $\sim 10$  MeV of pulsed gamma-ray emission which arises due to both ultrarelativistic primary particles (electrons) and cascades of secondary particles above polar caps of millisecond pulsars with dipolar magnetic fields of  $\sim 10^9$  G. In particular, we allow for different structures of the accelerating potential, and we show how this affects the slope of the predicted energy spectrum in the range of 100 MeV to 100 GeV. Also, Compton upscattering of ambient X-ray photons off ultrarelativistic electrons is taken into account. In Section 2 we present details of modelling the processes responsible for the formation of gamma-rays in millisecond pulsars. Section 3 describes spectral properties of two distinct components, due to curvature radiation (CR) and Compton scattering (ICS). Conclusions with a discussion of J0437-4715 come in Section 4.

## 2 THE MODEL OF HIGH-ENERGY RADIATION

We use a polar cap model, with most ingredients as postulated by Daugherty & Harding (1982) in context of classical pulsars. High-energy emission is a superposition of curvature radiation (CR) of ultrarelativistic primary electrons, and synchrotron radiation (SR) of secondary particles ( $e^\pm$  pairs) created via magnetic absorption of photons. Additional features include: 1) two models of electron acceleration, 2) inverse Compton scattering (ICS) of thermal X-ray photons on electrons. The first feature is important for the history of cooling of primary electrons and consequently it affects the slope of gamma-ray spectrum above 100 MeV. The second one (ICS) is not important for overall cooling of electrons, but the resulting TeV component in the gamma-ray spectra is of potential interest. A field of ambient photons necessary for the ICS is likely to be present within the magnetosphere of some millisecond pulsars, according to some interpretations of available X-ray and EUV observations (e.g. Zavlin & Pavlov 1998, Edelstein et al. 1995). We list the details of the model in the following subsections.

### 2.1 Geometry

We assume that the geometry of the magnetic field of a neutron star is well described by a static, axisymmetric dipole. In polar coordinates its field lines satisfy

$$r \sin^{-2} \theta = R_0, \quad (1)$$

where the dipole constant  $R_0$  defines a set of field lines which differ by azimuthal angle only. Polar caps are defined as (two) regions on the neutron star surface crossed by all lines for which the condition  $R_0 \geq R_{lc}$  is satisfied, where  $R_{lc} = cP/2\pi$  is a light-cylinder radius for a spin period  $P$ . The polar cap radius is then  $r_{pc} = R_{ns} \times (R_{ns}/R_{lc})^{1/2}$ , where  $R_{ns}$  is the radius of the neutron star for which we assume the canonical value of  $10^6$  cm. Beam particles (primary electrons) are ejected from the outer rim of the polar cap and move along the magnetic field lines.

When modelling an extended source of soft photons, which are to be targets for electrons in Compton scatterings, we consider two cases of its geometry. In the first case, the soft photons come from the hot polar cap with a uniform temperature  $T_{pc} \gtrsim 10^6$  K. In the second case the soft photons come from the entire surface of the neutron star, however now the temperature is lower:  $T_{surf} \gtrsim 10^5$  K.

### 2.2 Electron acceleration

Primary electrons are injected along magnetic field lines into the magnetosphere from the outer rim of the polar cap. The structure of longitudinal electric field responsible for their acceleration remains unknown. However, the electric field must be strong enough to ensure electron positron pair creation. The presence of pairs is a necessary condition for a magnetized neutron star to be a radio pulsar. Thus the requirement of creating pairs in the magnetosphere is the primary condition that the model has to satisfy.

We use two simple models for particle acceleration. The first one (denoted model A) assumes instant acceleration to ultrarelativistic energy  $E_e^{\text{init}}$  at the moment of electron injection on the surface of the neutron star. The values of  $E_e^{\text{init}}$  are set to be just above the threshold value for creation of secondary pairs  $E_e^{\text{min}}$  which in turn is a function of magnetic field strength at the polar cap  $B_{pc}$  and the spin period  $P$  (for details see Rudak & Dyks 1998, and Dyks 1998). For a pulsar with  $B_{pc} = 10^9$  G and  $P = 3$  ms, the initial energy is  $E_e^{\text{init}} = 1.07 \times 10^7$  MeV. For J0437-4715 we took  $B_{pc} = 7.4 \times 10^8$  G,  $P = 5.75$  ms, and  $E_e^{\text{init}} = 1.54 \times 10^7$  MeV, where we used the magnetic field derived from  $\dot{P}$  kinematically corrected by Camilo et al. (1994).

For comparison we consider another model (model B) of particle acceleration, in which the longitudinal electric field  $\mathcal{E}$  is set at a constant level with an exponential cutoff:

$$\mathcal{E} = \frac{V_0}{r_{pc}} \exp\left(-\frac{h}{r_{pc}}\right), \quad (2)$$

where the characteristic scale-height of the electric field is assumed to be equal to the radius of the polar cap  $r_{pc}$ . For a pulsar with  $B_{pc} = 10^9$  G and  $P = 3$  ms the value of  $\mathcal{E}$  at the polar cap surface was set at the level of  $V_0/r_{pc} \approx 10^9$  V cm $^{-1}$  to ensure a total yield of secondary pairs per primary electron similar to that in model (A). The initial value of the electron energy  $E_e^{\text{init}} = 10$  MeV was assumed.

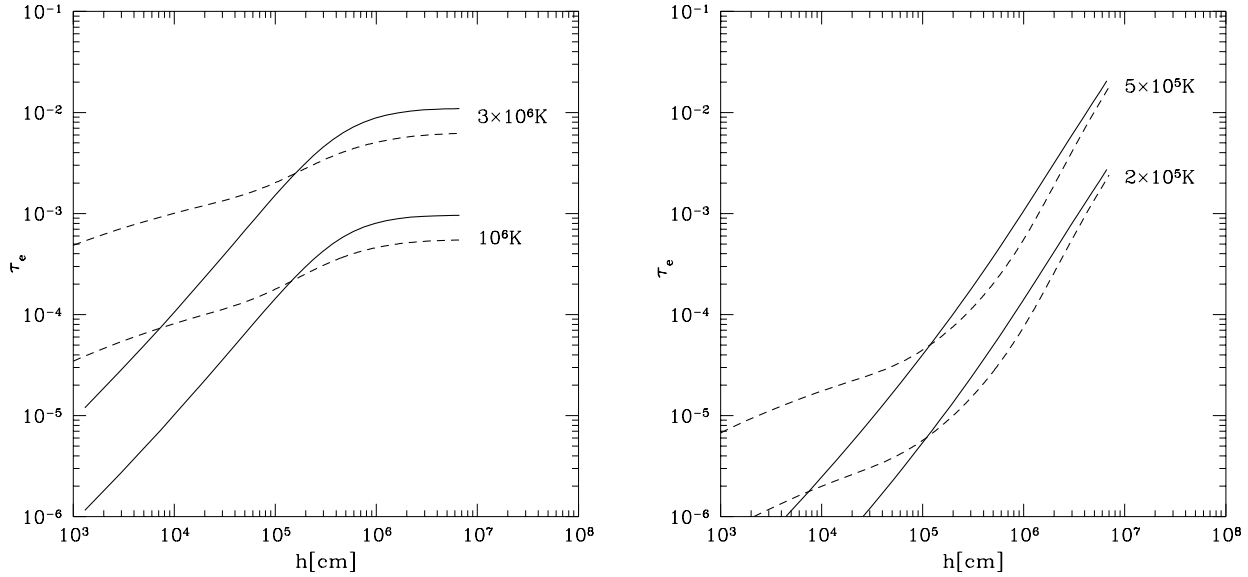


**Figure 1.** Cumulative optical depth  $\tau_e$  for non-magnetic scattering of an electron injected at the surface level ( $h = 0$ ) and crossing a blackbody radiation field. The left panel is for the radiation fields due to hot polar cap ( $T_{\text{cap}} = 10^6$  K and  $3 \times 10^6$  K). Solid lines are for instant acceleration with electron energy  $E_{\text{init}} = 10^7$  MeV. Dashed lines are for continuous acceleration in electric field  $\mathcal{E}$  (eq.2). The right panel is for the radiation fields due to hot stellar surface ( $T_{\text{surf}} = 2 \times 10^5$  K and  $5 \times 10^5$  K). The pulsar period is  $P = 3 \times 10^{-3}$  s and we used  $10^5$  electrons in the simulation.

As electrons accelerate they move along the magnetic field lines and are slowed down by the curvature radiation reaction. We calculate the electron energy budget as a function of the distance travelled in the magnetosphere. Only a small fraction (less than one percent, see Figure 1) of the electrons will scatter on thermal photons originating on the polar cap or on the stellar surface. Thus scattering is not an important electron deceleration process.

### 2.3 Curvature and synchrotron processes

We follow the model described by Rudak & Dyks (1999) who calculated broad band energy spectra of high-energy emission for two distinct pulsar groups: low-magnetic field pulsars (‘millisecond pulsars’) and classical pulsars.

The dominant cooling process for primary electrons is the curvature radiation:

$$(\dot{\gamma}_e)_{\text{cr}} = (2/3)\gamma_e^4 \rho^{-2} c r_0, \quad (3)$$

where  $\gamma_e$  is the electron Lorentz factor,  $\rho$  is the curvature radius, and  $r_0$  is the electron radius. When considering secondary electrons (pairs) one has to consider also the synchrotron radiation. The rate of SR cooling is

$$(\dot{\gamma}_e)_{\text{sr}} = -\frac{2}{3} \frac{r_0^2}{m_e c} B^2 \sin^2 \psi \gamma_e^2, \quad (4)$$

where  $\psi$  is the pitch angle of the pairs. The photon spectra due to curvature and synchrotron processes are calculated following Daugherty & Harding (1982). A detailed discussion of the role of these processes in the formation of gamma-ray spectra of pulsars is given in Rudak & Dyks (1999).

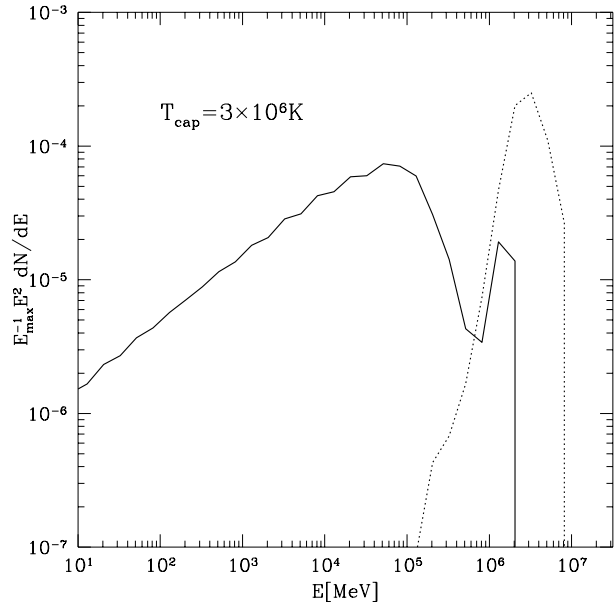


**Figure 2.** The dotted line shows the intrinsic spectrum of the inverse Compton photons i.e. with transfer effects neglected. The solid line shows the spectrum of magnetically reprocessed photons as seen by an external observer. Here we assumed: thermal emission from a polar cap with the temperature  $T_{\text{cap}} = 3 \times 10^6$  K, surface magnetic field  $B = 10^9$  G, pulsar period  $P = 3 \times 10^{-3}$  s, and instantaneous electron acceleration.

### 2.4 Scattering

Our numerical treatment of scattering process follows Daugherty & Harding (1989). As the electrons travel up in

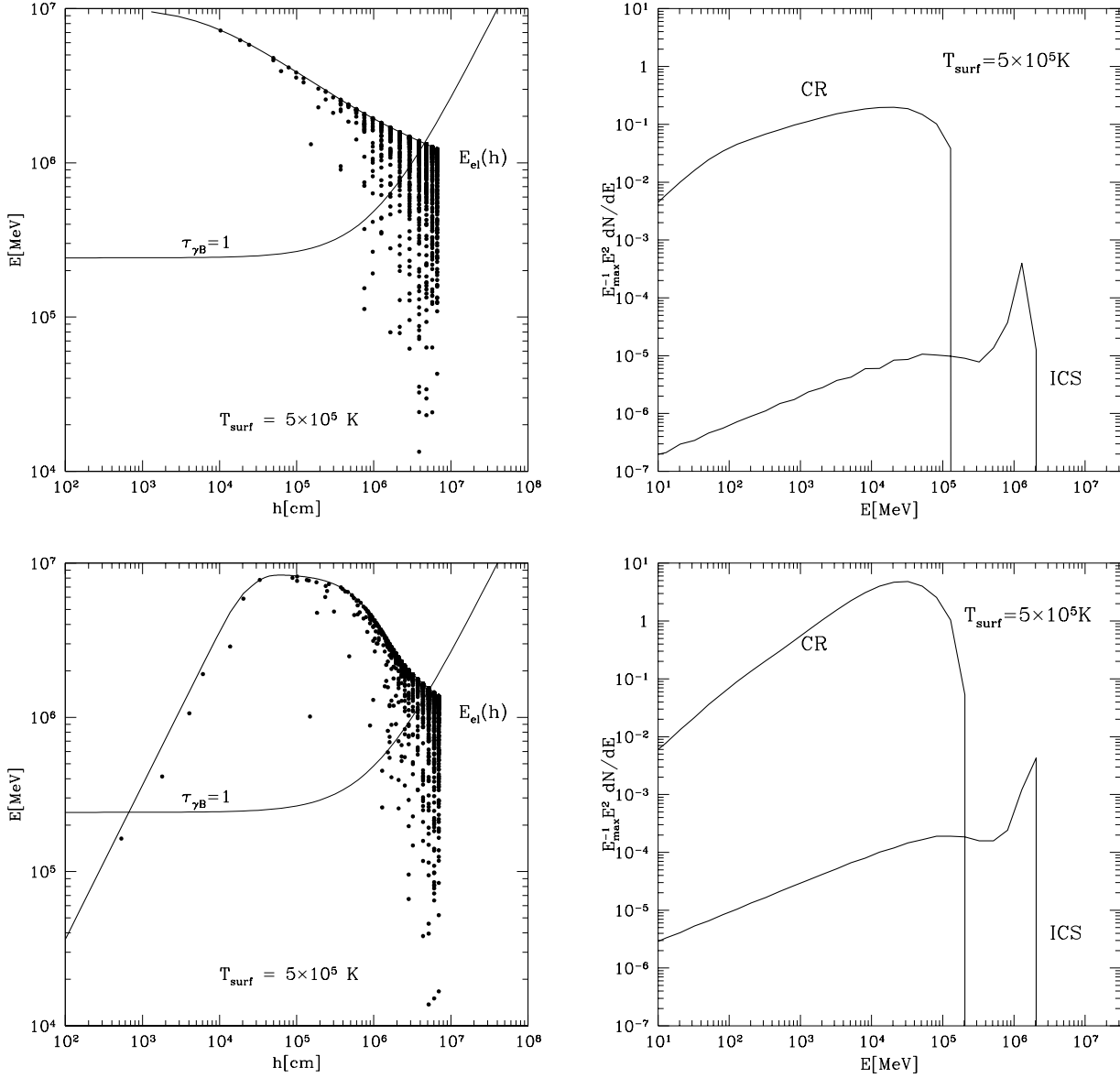


**Figure 3.** The thick solid lines in the left panels show the dependence of the mean energy of unscattered primary electrons as a function of the height. The top left panel corresponds to the case of instantaneous acceleration (model A), while the bottom left panel corresponds to case of acceleration described by eq. (2) (model B). The dots show the energies of the Compton upscattered photons and height where the scatterings took place (in these simulations we propagated  $10^5$  primary electrons in the magnetosphere). The thin solid line shows the optical depth to magnetic absorption equal to unity, according to equation (11). The right panels show the energy spectra formed for model A (top right panel) and model B (bottom right panel). The soft photons originate on the surface of the neutron star with the temperature  $T_{surf} = 5 \times 10^5$  K. The CR and the ICS spectral components are due to a single primary electron injected at the outer rim of the polar cap of the standard millisecond pulsar. We normalise the spectra with  $E_e^{max}$  - maximum energy of the electron, mediated between acceleration and cooling rates. For the top left panel,  $E_e^{max}$  is equal to the initial energy  $E_e^{init} = 1.07 \times 10^7$  MeV. Pulsar parameters are  $B_{pc} = 10^9$  G, and  $P = 3$  ms and  $E_e^{init} = 1.07 \times 10^7$  MeV for model A.

the magnetosphere they may scatter off thermal photons originating from the stellar surface or the polar cap. For millisecond pulsars the magnetic field at the surface is typically  $10^9$  G or less, i.e. much weaker than the critical field  $B_{crit} = 4.414 \times 10^{13}$  G. Thus the scattering process will be well described by the Klein-Nishina relativistic nonmagnetic cross section:

$$\sigma_{KN} = \frac{3\sigma_T}{4x} \left[ \frac{x^2 - 4x - 8}{x^2} \ln(1+x) + \frac{1}{2} + \frac{8}{x} - \frac{1}{2(1+x)^2} \right], \quad (5)$$

where:  $x = 2p^\nu k_\nu$ ,  $p^\nu$  is the electron four-momentum, and  $k_\nu$  is the photon four-wave vector. The scattering rate (in

the “lab frame”  $K$ ) by an electron travelling with velocity  $\vec{\beta}$  in a photon field is given by

$$\mathcal{R} = c \int d\Omega \int \varepsilon^2 d\varepsilon \sigma_{KN} f_\varepsilon (1 - \vec{\beta} \cdot \hat{n}_i) \quad (6)$$

where  $\Omega$  is the solid angle subtended by the source of soft photons,  $\sigma_{KN}$  is the total cross section,  $f_\varepsilon$  is the photon occupation density, and  $\hat{n}_i$  is the unit vector ( $\hat{n}_i \equiv \vec{k}/|\vec{k}|$ ) representing the direction of the incoming soft photon. Taking the Planck function for  $\varepsilon^2 f_\varepsilon$  this equation reads:

$$\mathcal{R} = \frac{c}{4\pi^3} \left( \frac{m_e c}{\hbar} \right)^3 \int d\Omega \int d\tilde{\varepsilon} \sigma_{KN} (1 - \vec{\beta} \cdot \hat{n}_i) \frac{\tilde{\varepsilon}^2}{\exp \tilde{\varepsilon}/\tilde{T} - 1} \quad (7)$$

where  $\tilde{\varepsilon}$  is the photon energy in the units of electron mass,  $\tilde{T}$  is the photon temperature in the units of electron mass.

We draw the energy and direction of the incoming photon from the distribution of  $\varepsilon^2 f_\varepsilon$ , and  $\Omega$ , respectively (as used in eq.6). Then we transfer them to the electron instantaneous rest frame  $K_e$  and there we find the photon scattering angle  $\theta$  using the Klein-Nishina differential cross section

$$\frac{d\sigma_{KN}}{d\mu d\phi} = \frac{3\sigma_T}{16\pi} \frac{1 + \mu^2}{\left[1 + \frac{\mu}{2}(1 - \mu)\right]^2} \times \left\{ 1 + \frac{x^2(1 - \mu)^2}{4(1 + \mu^2) \left[1 + \frac{\mu}{2}(1 - \mu)\right]} \right\}, \quad (8)$$

where  $\mu$  is the cosine of  $\theta$ . The energy  $\epsilon'$  of the scattered photon in  $K_e$  is obtained from the Compton formula

$$\epsilon' = \frac{\epsilon}{1 + \frac{\epsilon}{m_e c^2}(1 - \mu)}. \quad (9)$$

Finally, the energy of the outgoing photon is transformed back to  $K$ .

At each step, as the location of the electron changes, the solid angle  $\Omega$  is corrected for the finite size of the source of soft photons (the polar cap or the stellar surface). Thus, we take into account the effect of the decreasing photon number density with height (geometrical dilution) and then we calculate the scattering rate  $\mathcal{R}$  at a given height above the neutron star surface.

## 2.5 Magnetic photon absorption

Despite low magnetic field values, two conditions for the process of pair creation via magnetic photon absorption ( $\gamma + \vec{B} \rightarrow e^\pm$ ) - the energy threshold condition, and the high optical thickness  $\tau_{\gamma B}$  of the magnetosphere - may well be met in the context of millisecond pulsars. For instance, in the model spectra calculated numerically by Rudak & Dyks (1999) photons with the energy  $\sim 10^2$  GeV or higher were subject to the magnetic-absorption reprocessing.

In our simulations we use the absorption coefficient as described by Erber (1966):

$$\eta(\varepsilon) = \frac{1}{2} \frac{\alpha}{\lambda_c} \frac{B_\perp}{B_{crit}} T(\chi) \quad (10)$$

where  $\alpha$  is a fine structure constant,  $\lambda_c$  is a Compton wavelength,  $B_\perp$  is the component of the magnetic field perpendicular to the photon momentum, and  $\chi \equiv \frac{1}{2} \frac{B_\perp}{B_{crit}} \frac{\varepsilon}{m_e c^2}$  is the Erber parameter  $\chi$ . For the function  $T(\chi)$  we use its

approximation  $T(\chi) \approx 0.46 \exp(-4f/3\chi)$ , valid for  $\chi \lesssim 0.2$  (for  $\chi \gtrsim 0.2$  this approximation starts to overestimate  $\eta$ ). The function  $f$  is the near-threshold correction introduced by (Daugherty & Harding, 1983). In the case of millisecond pulsars equation (10) is a good approximation even with  $f = 1$ , since magnetic photon absorption occurs well above the threshold. Electron-positron pairs created through the magnetic absorption radiate then via the synchrotron process.

For demonstrative purposes it is useful to present the condition  $\tau_{\gamma B} \geq 1$  in an analytical way. It is straightforward to show that a photon created with a momentum parallel to the local magnetic field line at a height  $h$  above the neutron star surface will undergo magnetic absorption if its energy satisfies approximately the following inequality:

$$E \geq 10^5 \left( \frac{P}{10^{-3} \text{s}} \right)^{1/2} \left( \frac{B_{pc}}{10^9 \text{G}} \right)^{-1} \left( \frac{R_{ns}}{10^6 \text{cm}} \right)^{-1/2} \times \left( 1 + \frac{h}{R_{ns}} \right)^{5/2} \text{ MeV}. \quad (11)$$

This formula is valid for dipolar magnetic field, and the field line is attached to the outer rim of the polar cap, and it is in very good agreement with numerical calculations of magnetic photon absorption.

## 3 RESULTS

Electrons are either accelerated instantly (model A) or accelerated by the electric field given by equation 2 (model B), and decelerated mainly by the curvature radiation. In model B the deceleration rate is insignificant near the polar cap because it increases with the electron energy and  $E_e^{\text{init}}$  is small. On the other hand, the acceleration rate does not depend on the electron energy and it ceases at the height  $h \sim r_{pc}$  (eq.2). There exists a region in between where both competing processes balance. An example calculation of the electron energy is shown in Figures 3 and 4. The top left panel of each figure presents electron energy within model A, with  $E_e^{\text{init}} = 1.07 \times 10^7$  MeV. The bottom left panel shows the electron energy within model B; the electron reaches a maximum energy of a few TeV at the height  $h \simeq 4 \times 10^4$  cm (i.e.  $h/r_{pc} \simeq 1/6$ ).

The optical depth  $\tau_e$  for nonmagnetic scattering of an electron is small (Figure 1) and thus scattering is not a relevant deceleration process of electrons. The optical depth for scattering scales as  $\propto T^2$ , where  $T$  is the temperature of the radiation field. There are several factors that influence the scattering rate as a function of the height above the surface of the neutron star  $h$ . The photon density decreases with height, but the electron spends much more time in the upper part of the magnetosphere, thus increasing the chance of scattering there. We find that the latter effect is dominant and most of the scatterings take place in the upper part of the magnetosphere between  $10^5$  and  $10^7$  cm, where the electron energy is close to the value of a few TeV. This is illustrated in Figures 3 and 4 (left panels), where the electron energy is plotted as a function of  $h$ . We show the energies of the ICS photons and the locations of the scattering events. The intrinsic spectrum of the ICS photons has a width of about one decade in energy centered around a few TeV, corresponding to the range of electron energies in the region

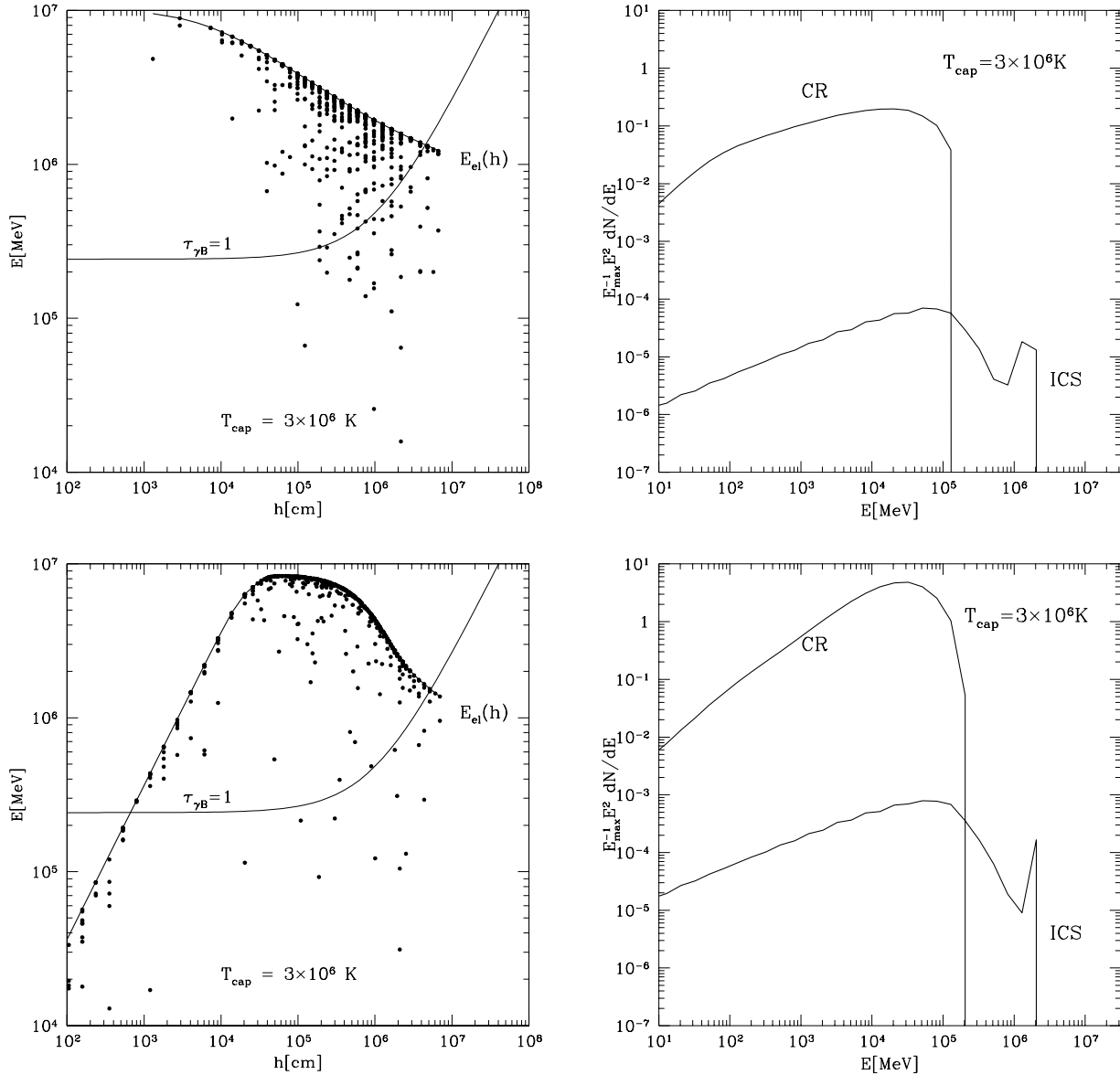


**Figure 4.** Same as Figure 3 but for the case of thermal emission from the polar cap with the temperature  $3 \times 10^6$  K.

where most of the scattering occur. In Figure 2 we illustrate the effects of reprocessing in the pulsar magnetosphere (taking model A as an example) and present both, the intrinsic spectrum of ICS photons (dotted line) and the spectrum after reprocessing due to magnetic absorption (solid line). Magnetic absorption removes the high energy part of the intrinsic ICS spectral peak, decreasing the strength of the peak by a factor of more than 10, and redistributing the ICS photon energy to lower part of the spectrum. The ICS photons subject to magnetic absorption reprocessing are located in Figures 3 and 4 (left panels) above the thin line corresponding to  $\tau_{\gamma B} = 1$  (equation [11]). In the case when the soft photon source is the hot polar cap most of the ICS photons will be reprocessed; see Figure 4. However, in the case when the photon source is a warm surface of a neutron star most of the scattering events take place at a distance of a few neutron star radii from the surface and most of the

ICS photons will escape freely; see Figure 3. The escaping ICS photons have typical energies equal to the electron energy at the height of few neutron star radii above the stellar surface and thus the spectrum of the ICS photons exhibits a strong peak at the energy of  $\approx 1$  TeV. The height of the ICS peak depends on the number of the soft thermal photons in the magnetosphere, and so it is directly related to the temperature and the radiating area (polar cap or entire stellar surface).

Another factor that influences the scattering rate is the soft photon flux anisotropy. Such anisotropy results from opacity angular dependence in strong magnetic field, and cannot be neglected in the case of classical pulsars with  $B \approx 10^{12}$  Gauss. Detailed models of magnetized atmospheres show that in the case  $10^9$  Gauss fields the soft photon flux is almost constant up to about 60 degrees (Pavlov

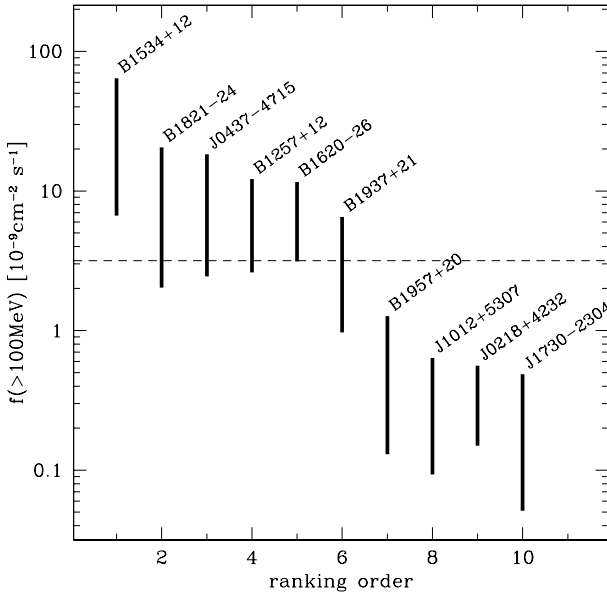


**Figure 5.** Millisecond pulsars ranked according to their gamma ray fluxes above 100 MeV expected within model A. Each vertical bar spans the range in the flux when the energy of injected primary electrons  $E_e^{\text{init}}$  varies by a factor of two. The horizontal dashed line represents the *GLAST* sensitivity.

et al., 1994). This result justifies our simplified treatment of the soft photon field as being isotropic.

The dominant spectral component in the energy range from 10 MeV out to its cutoff at  $\gtrsim 100$  GeV is due to curvature radiation (see the energy spectra in Figures 3 and 4, right panels). This cutoff energy is significantly higher than that expected in some classical pulsars as well as measured in some of them ( $\approx 10$  GeV, Thompson et al. (1997)). This is because of smaller curvature radii implying higher values of the characteristic photon energy, and also much weaker magnetic absorption ( $\gamma B \rightarrow e^\pm$ ). The slope  $\alpha$  of radiation energy spectrum per logarithmic energy bandwidth ( $E^2 dN/dE \propto E^\alpha$ ) below  $\epsilon_{\text{break}} \approx 100$  MeV is insensitive to model of acceleration, and is close to  $4/3$  (see Rudak & Dyks 1999 for discussion of  $\epsilon_{\text{break}}$ ). Above  $\sim 100$  MeV the spectrum assumes a slope which depends on the acceleration model. For model A the slope between 100 MeV and 10 GeV is  $1/3$ , in agreement with simple analytical estimates for monoenergetic source function of beam particles. The slope for model B was found numerically to be equal  $0.84$  (Bulik & Rudak, 1999). The electron acceleration in model B makes the electron spectrum harder in comparison to the case of model A, which in consequence leads to a harder CR spectrum. Note, that the total energy contained in gamma rays is larger in model B than in model A (compare right-hand panels of either Figure 3 or Figure 4). In model A the initial energy of electrons is large enough to enable pair creation, while in model B they need to overcome the CR losses to attain  $E_e^{\text{max}}$ . The work done by the electric field on the electron in model B is about 20 times larger than  $E_e^{\text{max}}$ .

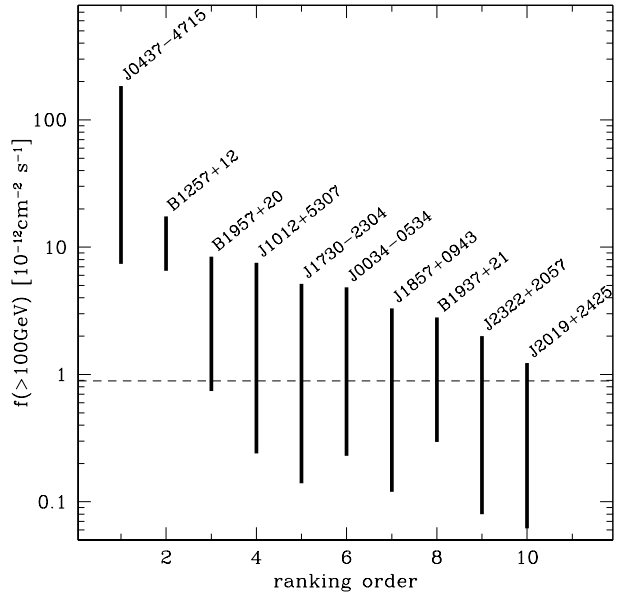


**Figure 6.** Similar to Fig.6 but the ranking is for gamma ray fluxes above 100 GeV, and the horizontal dashed line represents the *MAGIC* sensitivity.

#### 4 DISCUSSION

We calculated energy spectra of pulsed HE and VHE emission from millisecond pulsars for two models of beam particles acceleration. The spectra are a superposition of curvature (CR), synchrotron (SR), and Compton upscattering (ICS) components. The curvature component dominates the region between 1 MeV and 100 GeV. The slope of the spectrum in the range between 100 MeV and 10 GeV is sensitive to the details of the electron acceleration process. The synchrotron component becomes important only below  $\sim 1$  MeV (Rudak & Dyks 1999). The ICS component has a narrow peak around 1 TeV and its strength is related to the number density of the soft photons in the magnetosphere. Two sources of soft photons were considered: the hot polar cap with a uniform temperature  $T_{\text{pc}} \gtrsim 10^6$  K, and the entire surface of the neutron star, with a lower temperature:  $T_{\text{surf}} \gtrsim 10^5$  K.

Several new gamma-ray telescopes will be operational in the near future (Weekes, 1999) and thus it is interesting to discuss the observability of the HE radiation from millisecond pulsars. For our ranking we have selected the millisecond pulsars from the pulsar catalog of Taylor et al. (1995) using the following criteria  $P < 60$  ms and  $\dot{P} < 10^{-17}$ . For each pulsar the expected integral fluxes above 100 MeV and above 100 GeV was then calculated. Model A had been chosen for these calculations as a more conservative one. Moreover, two cases were considered for each pulsar: in addition to the case with the energy of injected primary electrons  $E_e^{\text{init}}$  being chosen according to section 2.2 (see also eq.8 of Rudak & Dyks 1998), we also allowed the electron energy to be two times higher. This was done to present how sensitive the results are to our choice of the electron's energy. We used the results of Rudak & Dyks (1998) to calibrate the fluxes of primary electrons (note that the spectra pre-

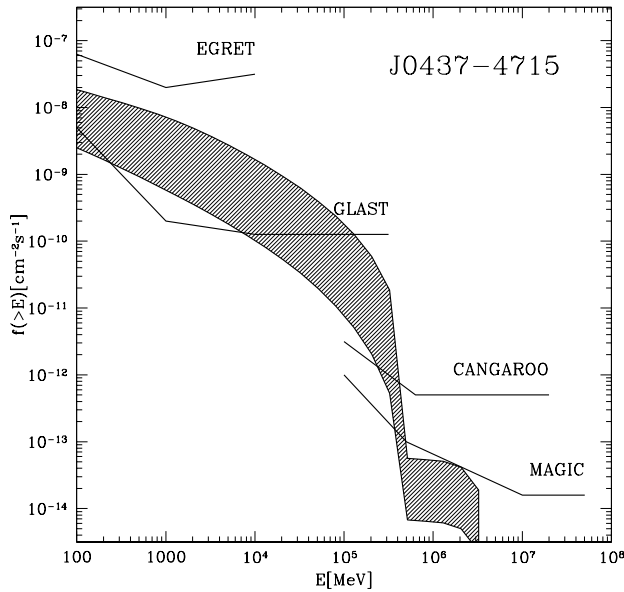


**Figure 7.** Integral spectral fluxes of photons calculated for J0437-4715 at the distance of 140 pc. Model A is used with two following values of  $E_e^{\text{init}}$ : 1)  $1.54 \times 10^7$  MeV (after Rudak & Dyks 1998, see also section 2.2), 2) a value two times higher, i.e.  $3.08 \times 10^7$  MeV. These two values give the spectra (solid lines) which limit the shaded region from the bottom and the top, respectively. The soft photons used for ICS come from the entire stellar surface with the temperature  $4 \times 10^5$  K (Edelstein et al., 1995). Sensitivities of several high energy detectors are also indicated.

sented in Figures 3 and 4, are per single electron). Ten best candidates in each band are presented in Figures 5 and 6 respectively. The first two candidates for GLAST observations (Figure 5), B1534+12 and B1821-24, are objects with relatively high magnetic fields, which place them in a transition region between the domains of classical and millisecond pulsars. Because of the magnetic field strength and consequently high magnetic absorption in these two objects, the high energy cutoff lies below 100 GeV and therefore they disappear from the ranking of Figure 6.

The third best candidate for GLAST observations is J0437-4715, a pulsar located very close to the Earth at the distance of 140 pc, with the spin period  $P = 5.75$  ms, and the magnetic field at the polar cap  $B_{\text{pc}} = 7.4 \times 10^8$  G inferred from kinematically corrected  $\dot{P}$  (Camilo et al., 1994). J0437-4715 is also our primary candidate for observations in the range above 100 GeV with the future Cherenkov telescopes. The integral photon spectra of J0437-4715 obtained in the course of calculations for the purposes of the ranking are presented in Figure 7 along with the sensitivities of GLAST, CANGAROO, as well as MAGIC in its ‘Large Zenith Angle’ mode. The expected photon flux in the *EGRET* energy range (i.e. between 0.1 and 10 GeV) is between  $\approx 2.0 \times 10^{-9} \text{ cm}^{-2} \text{ s}^{-1}$ , and  $\approx 2 \times 10^{-8} \text{ cm}^{-2} \text{ s}^{-1}$  (for  $E_e^{\text{init}} = 1.54 \times 10^7$  MeV and  $E_e^{\text{init}} = 3.08 \times 10^7$  MeV, respectively) and falls below the upper limit of  $2.1 \times 10^{-7} \text{ cm}^{-2} \text{ s}^{-1}$  placed with *EGRET* for this object (Fierro et al., 1995). Figure 7 shows that the flux expected from J0437-4715 in the

*GLAST* energy range (0.1 to 200 GeV) is above its sensitivity limit of  $3 \times 10^{-9} \text{ cm}^{-2} \text{ s}^{-1}$  (Kamae et al., 1999).

In the list of potential targets for atmospheric Cherenkov telescopes, presented in Figure 6, J0437-4715 clearly stands out as the strongest source, mainly because of its proximity. The next source B1257+12 is also rather strong and should be detected by the telescopes in the northern hemisphere like MAGIC and VERITAS, and also it could be seen by CANGAROO-III. The remaining objects have the expected fluxes between a few times  $10^{-13}$  and a few times  $10^{-12} \text{ cm}^{-2} \text{ s}^{-1}$ , which places them in a class of possible but uncertain targets.

The 100 GeV part of J0437-4715 spectrum can be probed by Cherenkov telescopes in the southern hemisphere like CANGAROO-III. This object should be also visible just above the horizon by the *MAGIC* telescope in the Canary Islands. The expected photon flux above 100 GeV is  $\approx 10^{-10} \text{ cm}^{-2} \text{ s}^{-1}$  which is almost two orders of magnitude above the sensitivity of *MAGIC* in its Large Zenith Angle mode (Blanch et al., 1998). *MAGIC* may also probe the ICS component of the spectrum (above 0.5 TeV) provided the energy of beam particles (i.e. primary electrons) is higher than assumed in our model.

Our ranking list of Figure 5 also includes J0218+4232, a pulsar with a likely detection by *EGRET* at about  $3\sigma$  level (Verbunt et al. 1996, Kuiper & Hermesen 2000). Our theoretical gamma ray flux for this object is a factor of up to ten below the expected *GLAST* sensitivity, mainly because of the large distance. Thus within the model presented above we remain skeptical to this report about its positive detection, knowing that the gamma ray source is coincident with an AGN.

Millisecond pulsars are potentially very interesting sources of high energy gamma-rays. The gamma-ray radiation, if detected, shall provide useful information about physical conditions in a pulsar magnetosphere: the primary electron energy, the nature of the electric field accelerating the primary electrons, and indirectly soft photon density. We appeal to include the millisecond pulsars into target lists for the upcoming gamma-ray observatories, both space- and ground-based.

## ACKNOWLEDGMENTS

This research has been supported by KBN grant 2P03D02117. We thank Gottfried Kannbach for useful discussions on gamma-ray detectors. Insightful comments and suggestions made by an anonymous referee allowed us to improve considerably the presentation of the paper.

## REFERENCES

- Becker W. & Trümper J., 1997, A&A, 326, 682
- Becker W. & Trümper J., 1999, A&A, 341, 803
- Blanch O., Blanchot G., Bosman M., et al., 1998, The MAGIC telescope, Letter of Intent
- Bulik T. & Rudak B., 1999, Proc. of the 3rd INTEGRAL Workshop
- Camilo F., Thorsett S.E., & Kulkarni S.R., 1994, ApJ, 421, L15
- Carraminana A., Bennett K., Buccheri R., et al., 1995, A&A, 304, 258



- Daugherty J.K. & Harding A.K., 1982, ApJ, 252, 337  
Daugherty J.K. & Harding A.K., 1983, ApJ, 273, 761  
Dermer C.D. & Sturmer S.J., 1994, ApJ, 420, L75  
Dyks J., 1998, Acta Astronomica, 48, 355  
Edelstein J., Foster R.S., & Bowyer S., 1995, ApJ, 454, 442  
Fierro J.M., Arzoumanian Z., Bailes M., et al., 1995, ApJ, 447, 807  
Kamae T., Ohsugi T., Thompson D., & Watanabe K., 1999, in *astro-ph/9901187*  
Kuiper L. & Hermesen W., 2000, Proceedings of the 177 IAU Symposium, Bonn  
Pavlov G.G., Shibano Y.A., Ventura J., & Zavlin V.E., 1994, A&A, 289, 837  
Rudak B. & Dyks J., 1998, MNRAS, 295, 337  
Rudak B. & Dyks J., 1999, MNRAS, 303, 477  
Sturmer S.J. & Dermer C.D., 1994, A&A, 281, L101  
Taylor J.H., Manchester R.N., Lyne A.G., & Camilo F., 1995, <http://pulsar.princeton.edu>  
Thompson D.J., Harding A.K., Hermesen W., & Ulmer M.P., 1997, in *AIP Conf. Proc. 410: Proceedings of the Fourth Compton Symposium*, 39  
Weekes T., 1999, High energy astrophysics, astro-ph/9903263  
Wei D.M., Cheng K.S., & Lu T., 1996, ApJ, 468, 207